Study of Giant Edge-Localized Modes in DIII-D and Comparison with Ballooning Theory

P. Gohil, M. Ali Mahdavi, L. Lao, K. H. Burrell, M. S. Chu, J. C. DeBoo, C. L. Hsieh, N. Ohyabu,
R. T. Snider, R. D. Stambaugh, and R. E. Stockdale

General Atomics, San Diego, California 92138
(Received 2 May 1988)

In DIII-D *H*-mode plasmas, large amplitude modulation of steep-edge electron-pressure gradients are observed during the occurrences of giant edge-localized modes (ELM's). For a considerable range of plasma currents (1 to 2 MA), the experimental pressure gradient before a giant ELM is close to the theoretically predicted marginal stability limit for the first regime of the ideal ballooning mode. These results, together with observations showing that ELM's originate in the region of bad curvature, strongly suggest that ELM's are triggered by ballooning mode instabilities.

In tokamaks, the existence of a phase of improved confinement during auxiliary heating, known as *H* mode, has shown a path toward obtaining higher global particle and energy confinement.[1-4] Edge MHD instabilities known as edge-localized modes (ELM's) generally tend to degrade particle and energy confinement at the plasma edge and inhibit increases in the plasma density.[5] During ELM's in DIII-D, tens of megawatts of power (between 10% and 20% of the stored energy) can be dumped to the divertor plates compared to only 1-2 MW of power flow during the ELM-free periods.[6,7] The study of the plasma edge, especially with regard to local electron density and temperature profiles, is important in elucidating the causes of, and thereby controlling, the ELM's. The presence of steep-edge electron density and temperature gradients are general characteristics of the *H* mode[2,8] and believed to be the result of a transport barrier at the edge.[9] In DIII-D, we have observed extremely steep-edge density gradients and correspondingly high-edge electron-pressure gradients. In the present work, we propose a relationship between the edge plasma parameters and MHD instabilities, specifically ballooning instabilities.

Our first investigation was to obtain detailed time histories of the edge electron density and temperature profile for a fixed set of DIII-D operating parameters: plasma current, $I_p = 1.25$ MA; toroidal magnetic field, $B_T = 2.1$ T; diverted deuterium discharges of minor radius, $a = 0.64$ m; major radius, $R = 1.69$ m; preneutral beam-injection Ohmic line-averaged density, $\bar{n}_e = 3.4 \times 10^{19}$ m^{-3}. Gas puffing was turned off during the neutral-beam injection (NBI). The discharges were auxiliary heated by a 75-keV neutral hydrogen beam injection at a typical power of 6.8 MW and 1-s pulse duration. The separation between the wall and limiters and the last enclosed plasma flux surface, the separatrix, was about 0.03 m everywhere. The *X*-point height above the divertor plates was kept constant at 0.20 ± 0.01 m.

To study the temporal evolution of the plasma-edge profiles, Thomson scattering was performed during 45

repeated, reproducible discharges with the laser timing varied from shot to shot. The Thomson-scattering system for DIII-D produces a 28-point spatially resolved electron density and temperature profile per laser pulse during a plasma discharge. The ruby laser beam is pro-
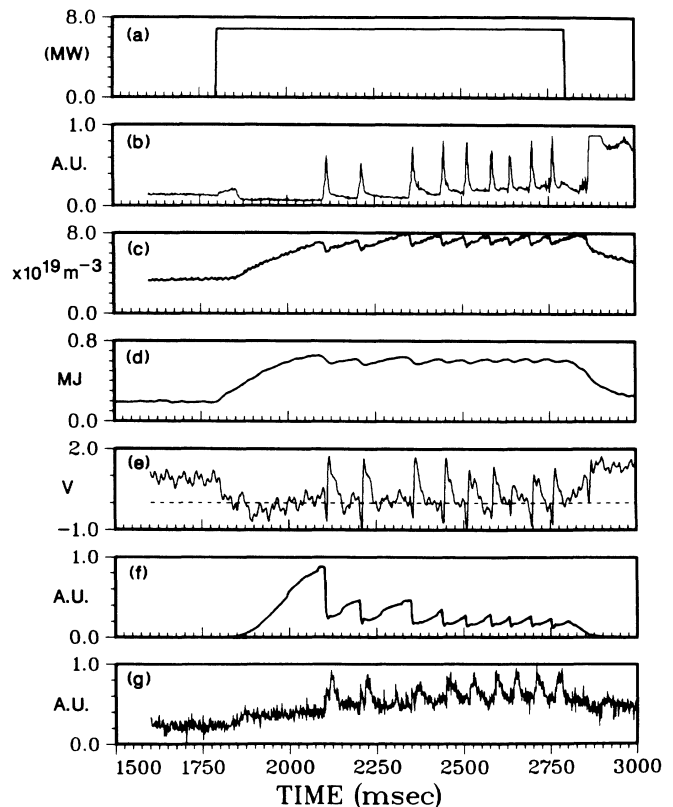
FIG. 1. Time histories from a typical *H*-mode discharge with giant ELM's for 1.25-MA plasma current, 2.1-T toroidal field, NBI power of 6.8 MW, (a) NBI power, (b) D_α emission in the divertor region, (c) line-averaged electron density, (d) plasma stored energy, (e) loop voltage, (f) edge soft x-ray emission, and (g) edge visible bremsstrahlung.

jected vertically through the plasma along a chord about 0.17 m radially outward from the magnetic axis of the plasma studied. Measurements from various diagnostic systems [e.g., soft x-ray photodiodes, deuterium emission (D_α) photodiodes, charge-exchange-recombination spectroscopy, vacuum-ultraviolet spectroscopy, Langmuir probes, bolometer, CO_2 interferometry, magnetics, visible bremsstrahlung], especially those observing the plasma edge, were carefully monitored to check on discharge reproducibility. The spatial location of the separatrix in the region of the scattering measurements was determined to an accuracy of ± 1 cm from magnetic measurements combined with a full MHD equilibrium analysis.[10]

Edge profile data were obtained from 250 ms before to 300 ms after the L-H transition; this period also included the first giant ELM. The giant ELM's are characterized by a very fast increase in the D_α emission followed by a slower decay and typically last for 10 ms. The H mode studied exhibited the normal characteristics of increased

line-averaged density, sharp reduction in D_α emission at the divertor and midplane regions, increase in plasma stored energy, and reduced power flow across the separatrix into the divertor. Figure 1 shows time traces of these quantities for a standard discharge.

The electron density, temperature, and pressure gradients attained steady values by 100 ms after the L-H transition. Figure 2 shows the electron density and temperature profiles 5 ms before and 11 ms after the start (i.e., the leading edge) of the ELM. The electron temperature profile tended to form a pedestal near the edge of the plasma (typically starting at ~ 3 cm radially inside the separatrix), which exhibited no discernible change immediately prior to the ELM and was consistently around 300 eV. However, immediately after the ELM, the edge-electron temperature pedestal is lower at around 220 eV. The error in the measurement was 30 eV, which is based on a combination of the minimum temperature resolution of the spectrometer and systematic shot-to-shot fluctuations of the signal in the detector chain. The edge-electron temperature gradient is calculated from measurements made vertically along the laser beam and transformed to radial coordinates corresponding to the same poloidal flux surfaces, which were determined from a MHD fit to magnetic data. The plasma pressure was assumed to be constant over a given flux surface.

The edge-electron pressure gradient appears to peak just before the ELM and to be dramatically reduced by the ELM as shown in Fig. 3. The electron density plays
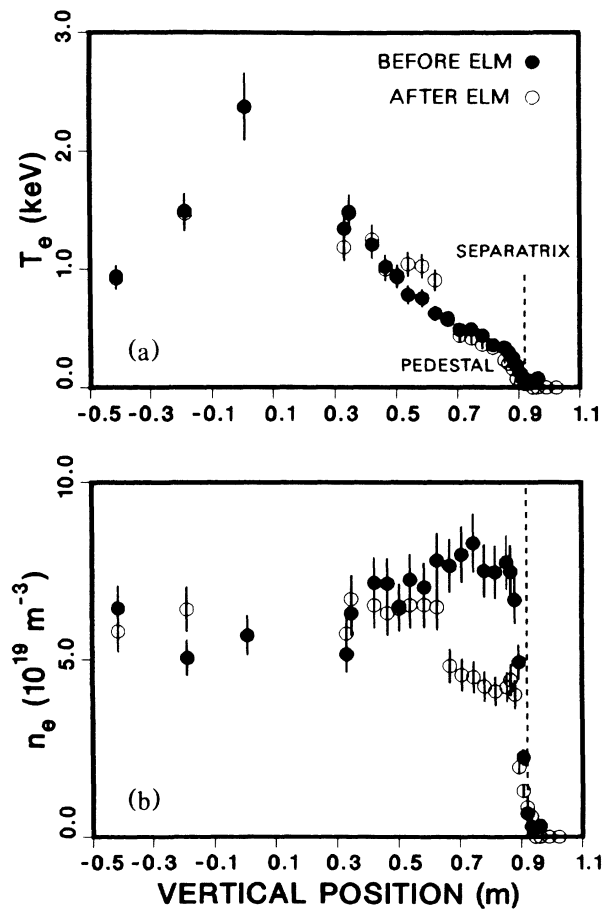
FIG. 2. (a) Electron temperature profile and (b) electron density profile 5 ms before (●) and 11 ms after (○) the start of the first giant ELM ($I_p = 1.25$ MA; $B_T = 2.1$ T; $P_{BEAM} = 6.8$ MW).
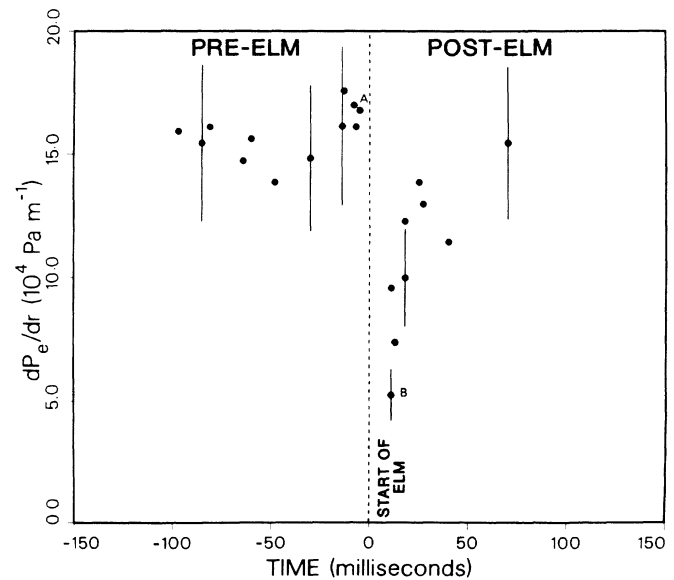
FIG. 3. The edge-electron pressure gradient as a function of time before and after the start (i.e., the leading edge) of the first giant ELM. The data points A and B correspond to the profiles before and after the ELM, respectively, shown in Fig. 2.

the major role in contributing to the changes in the pressure gradient during the ELM. The edge-electron density gradient is constant around 3.2×10^{21} m^{-4} prior to an ELM, but is decreased to about 1.5×10^{21} m^{-4} at 11 ms after the start of the ELM. Correspondingly, the electron pressure gradient is about 1.7×10^5 Pa m^{-1} immediately prior to the ELM, but decreases to about 5.3×10^4 Pa m^{-1} 11 ms after the start of the ELM. In both cases, the scale length for the largest gradient is 2 cm, radially within the separatrix. The ELM timing with respect to the laser was too random to obtain a profile measurement directly at the onset of the ELM, that is, at the peak of the D_α emission. It is suspected that the edge-electron density and pressure gradients will be even lower at the ELM peak, that is, even lower than the measured pressure gradients just after an ELM (see Figs. 3 and 4). The reduction in the edge pressure gradient predominantly results from the decrease in the edge-electron density as a result of the expulsion of particles from the plasma edge within 23 cm radially from the separatrix. Both the electron density and pressure gradients recover to their respective pre-ELM values within 50 ms after the start of the ELM.

Our observed large pressure gradients led us to compare our data to Bishop's theory of H mode[11] in which Bishop pointed out that a proper orientation of the separatrix can facilitate the coalescence of the first and second stability regions. Bishop also showed that if the plasma current density near the edge were to exceed a critical value, the edge plasma would have access to the second stable regime for ballooning modes and that this

entry into the second stable regime might be the $L \rightarrow H$ transition. Figure 4 is a diagram of our data constructed in the style of Bishop's ballooning stability diagrams. Clearly, when a threshold in edge temperature is exceeded (the L-H transition), the pressure gradient increases dramatically. However, the highest pressure gradient, just before an ELM, only reaches the *first stable regime ballooning limit*. Moreover, the figure also shows that the ELM essentially modulates the pressure gradient between the ballooning limit and the L-mode value. The time constants for the increase in the pressure gradient after the L-H transition and after an ELM are similar. These observations led us to the hypothesis that the L-H transition is not connected to ideal ballooning modes at the second stability boundary, but that the ELM may be a short transient relapse into L mode triggered by the edge pressure gradient hitting the first stable regime ballooning limit.

The marginal stability limit for the first regime of ballooning mode theory was calculated with the ideal MHD stability codes, MBC[12,13] and CAMINO.[14] These codes solve the full 2D ballooning equation in the exact toroidal geometry. To find the marginal pressure limit, the pressure profile in the initial equilibrium is continuously modified, according to the analytical scheme given in Ref. 13, until the growth rate of the mode vanishes. The plasma equilibrium is determined by an MHD equi-

FIG. 4. The edge-electron pressure gradient during Ohmic heating, L mode, and H mode (pre-ELM) and after the first giant ELM as a function of the edge-electron temperature at the temperature pedestal.
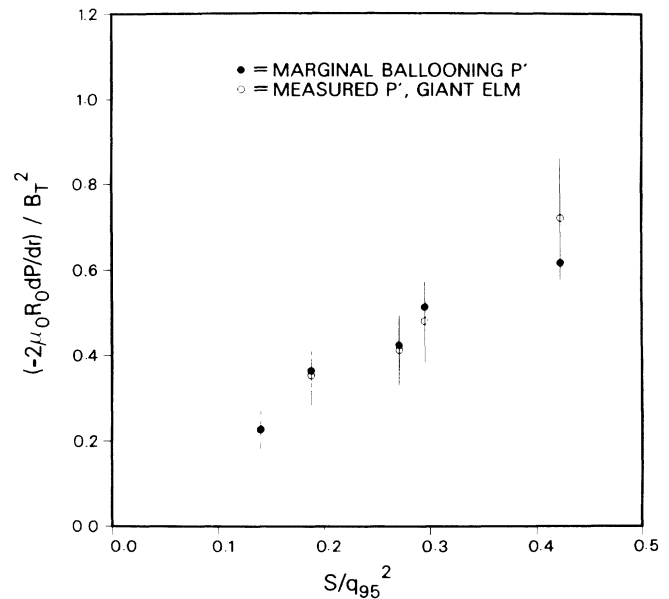
FIG. 5. The edge-electron pressure gradient as a function of S/q^2 at 95% of the enclosed poloidal flux. The data points correspond to deuterium discharges with varying plasma currents (from 1.0 to 2.0 MA) and neutral hydrogen beam injection. The range of NBI powers was 5.8 to 8.7 MW with the higher powers prevalent at the higher currents. The prebeam Ohmic line-averaged electron density varied from 2.5×10^{19} m^{-3} for the 1.0-MA case to 5×10^{19} m^{-3} for the 2-MA case.

librium fitting code, EFIT,[10] from experimentally measured kinetic profiles and magnetic data. The stability code calculates the total pressure gradient at the marginal stability limit and the limit for the electron pressure gradient is taken to be one-half of the total with the assumption that $T_i = T_e$ as indicated by measurements of the ion temperature profiles from charge-exchange-recombination spectroscopy. Analysis with the ONETWO[15] transport code showed that the fast-ion contribution to the pressure from the neutral beams was less than 5%. The stability limit was evaluated for the flux surface at 95% of the poloidal flux enclosed inside the separatrix. The limit is not very sensitive to the separation of the flux surface from separatrix. The measured pressure gradients prior to the occurrence of the giant ELM are in the first region of the calculated stability limit.

The measured pressure gradients before ELM for discharges ranging in plasma current from 1 to 2 MA are within 1 standard deviation of the theoretically predicted marginal stability limit for the first regime of the ideal ballooning mode. Figure 5 shows the measured edge-electron pressure gradient together with the theoretically predicted marginal stability limit as a function of S/q^2 at 95% of the enclosed flux surface, where S is the shear and q is the safety factor. These data points include additional data from a different set of discharges (see figure caption) to the reproducible discharges described earlier, which were taken for a fixed set of run parameters. The increase in the experimental pressure gradients with current is predominantly due to the increase in the edge-electron density rather than the electron temperature. The linear relationship of the pressure gradient with S/q^2 is consistent with the ideal ballooning mode instability. These results strongly suggest that giant ELM's are triggered by ballooning instabilities.

The onset of the D_α emission at the outside midplane, which is the region most susceptible to ballooning instability, and at the outside divertor plates precedes that at the inside divertor plates by 200 μs which is consistent with the ELM occurring initially at the outside midplane and then propagating poloidally at approximately the ion sound velocity along the plasma periphery.[6]

In summary, very steep-electron-pressure gradients have been observed in the boundary of H-mode plasmas. Over a wide range of plasma parameters, the edge pressure gradient is at the limit for marginal stability of the ideal ballooning mode before the occurrence of an ELM. The temporal evolution of the D_α emission along the plasma periphery and the heat pulses at the divertor plates are consistent with the ELM originating at the outside midplane. These observations strongly suggest that ELM's are triggered by the ideal ballooning mode. Further, the edge pressure gradients in H mode remain in the first stable regime of ballooning mode theory over a wide range of plasma currents.

An important implication of the result that the pressure gradient in the region of improved confinement is limited by the ideal-ballooning-mode limit is that the energy confinement of the H-mode plasmas may be ultimately limited by the ballooning mode. Therefore, plasma-shaping techniques used for β optimization may also lead to improved plasma confinement.

[1]F. Wagner et al., Phys. Rev. Lett. 49, 1408 (1982).

[2]S. M. Kaye et al., J. Nucl. Mater. 121, 115 (1984).

[3]K. H. Burrell et al., Phys. Rev. Lett. 59, 1432 (1987).

[4]A. Tanga et al., Nucl. Fusion 27, 1877 (1987).

[5]F. Wagner et al., J. Nucl. Mater. 121, 103 (1984).

[6]D. Hill et al., Nucl. Fusion 28, 902 (1988).

[7]M. Ali Mahdavi et al., General Atomics Report No. GA-A18909, 1987 (unpublished).

[8]M. Keilhacker et al., Plasma Phys. Controlled Fusion 26, 49 (1984).

[9]M. Keilhacker et al., Plasma Phys. Controlled Fusion 28, 29 (1986).

[10]L. L. Lao et al., Nucl. Fusion 25, 1611 (1985).

[11]C. M. Bishop, Nucl. Fusion 26, 1063 (1986).

[12]R. W. Moore, General Atomics Report No. GA-A16243, 1981 (unpublished).

[13]J. M. Greene and M. S. Chance, Nucl. Fusion 21, 453 (1981).

[14]M. S. Chance, in Theory of Fusion Plasmas, edited by A. Bondeson, E. Sindoni, and F. Troyon (Società Italiana di Fisica, Bologna, Italy, 1988), p. 87.

[15]W. W. Pfeiffer et al., General Atomics Report No. GA-A16178, 1980 (unpublished).